IMMUNE NETWORK

Original Article

Check for updates

The Immunosuppressive Potential of Cholesterol Sulfate Through T Cell Microvilli Disruption

Jeong-Su Park [1,2], Ik-Joo Chung[3], Hye-Ran Kim [1,2,4,*], Chang-Duk Jun [1,2,*]

[1]School of Life Sciences, Gwangju Institute of Science and Technology (GIST), Gwangju 61005, Korea
[2]Immune Synapse and Cell Therapy Research Center, Gwangju Institute of Science and Technology (GIST), Gwangju 61005, Korea
[3]Department of Hematology-Oncology, Immunotherapy Innovation Center, Chonnam National University Medical School, Hwasun 58128, Korea
[4]Division of Rare and Refractory Cancer, Tumor Immunology, Research Institute, National Cancer Center, Goyang 10408, Korea

*Correspondence to
Chang-Duk Jun
School of Life Sciences and Immune Synapse and Cell Therapy Research Center, Gwangju Institute of Science and Technology (GIST), 123 Cheomdangwagi-ro, Buk-gu, Gwangju 61005, Korea.
Email: cdjun@gist.ac.kr

Hye-Ran Kim
Division of Rare and Refractory Cancer, Tumor Immunology, Research Institute, National Cancer Center, 323 Ilsan-ro, Ilsandong-gu, Goyang 10408, Korea.
Email: hrkim@ncc.re.kr

ORCID iDs
Jeong-Su Park
https://orcid.org/0000-0002-8710-0455
Hye-Ran Kim
https://orcid.org/0000-0001-6854-4774

ABSTRACT

Cholesterol (CL) is required for various biomolecular production processes, including those of cell membrane components. Therefore, to meet these needs, CL is converted into various derivatives. Among these derivatives is cholesterol sulfate (CS), a naturally produced CL derivative by the sulfotransferase family 2B1 (SULT2B1), which is widely present in human plasma. CS is involved in cell membrane stabilization, blood clotting, keratinocyte differentiation, and TCR nanocluster deformation. This study shows that treatment of T cells with CS resulted in the decreased surface expression of some surface T-cell proteins and reduced IL-2 release. Furthermore, T cells treated with CS significantly reduced lipid raft contents and membrane CLs. Surprisingly, using the electron microscope, we also observed that CS led to the disruption of T-cell microvilli, releasing small microvilli particles containing TCRs and other microvillar proteins. However, *in vivo*, T cells with CS showed aberrant migration to high endothelial venules and limited infiltrating splenic T-cell zones compared with the untreated T cells. Additionally, we observed significant alleviation of atopic dermatitis in mice injected with CS in the animal model. Based on these results, we conclude that CS is an immunosuppressive natural lipid that impairs TCR signaling by disrupting microvillar function in T cells, suggesting its usefulness as a therapeutic agent for alleviating T-cell-mediated hypersensitivity and a potential target for treating autoimmune diseases.

Keywords: T cells; Cholesterol; Cholesterol sulfate; Cell microvilli disruption; Autoimmune disease

INTRODUCTION

Cholesterol (CL) is one of the essential biosynthetic molecules that make up organisms. It forms part of the biological membranes and account for these cell membranes' fluidity (1). CL is also used as a precursor material in hormone synthesis (2). Moreover, CL can bind to the TCR β chain (3) and compartmentalize the subdomains of the plasma membrane called "lipid rafts" (4). Subsequently, lipid rafts can amplify T cell signaling by ordering signaling

Chang-Duk Jun
https://orcid.org/0000-0002-1372-9277

Conflict of Interest
The authors declare no potential conflicts of interest.

Abbreviations
AD, atopic dermatitis; APC, Ag-presenting cell; BMDC, bone marrow-derived dendritic cell; CL, cholesterol; CS, cholesterol sulfate; c-SMAC, central-supramolecular activation clusters; CTB, cholera toxin subunit B; DAB, 3,3'-diaminobenzidine; DC, dendritic cell; HEV, high endothelial venule; i.v., intravenously; IHC, immunohistochemistry; IO, ionomycin; LDL, low-density lipoprotein; LN, lymph node; MβCD, methyl-β-cyclodextrin; NS, not significant (p>0.05); NT, nontreated T cells; OVA, ovalbumin; PLL, poly-L-lysine; PMA, phorbol 12-myristate 13-acetate; qPCR, quantitative PCR; RT, room temperature; s.c., subcutaneously; SULT2B1, sulfotransferase family 2B1; TBS-T, TBS containing 0.1% Tween 20; TEM, transmission electron microscopy; TNBC, 2,4,6-trinitrochlorobenzene.

Author Contributions
Conceptualization: Park JS, Chung IJ, Kim HR, Jun CD; Data curation: Kim HR; Formal analysis: Park JS; Investigation: Kim HR; Methodology: Park JS, Chung IJ, Kim HR, Jun CD; Project administration: Park JS; Resources: Chung IJ; Supervision: Jun CD, Kim HR; Validation: Park JS, Kim HR, Jun CD; Writing - original draft: Park JS, Kim HR, Jun CD; Writing - review & editing: Jun CD, Kim HR

molecules when T cells are stimulated (5). Thus, the depletion of CL disrupts lipid rafts, resulting in impaired TCR signaling (6,7). Under unique *in vivo* conditions, studies have shown that CL is also converted to derivatives by many enzymes for oxidation, sulfation, and esterification (8-10). For instance, 25-hydroxycholesterol, an oxysterol produced by CL oxidase, increases inflammatory reactions (11), whereas 7β-hydroxycholesterol causes apoptosis by regulating the movement of Ca^{2+} ions in human aortic smoothed muscle cells (12).

Cholesterol sulfate (CS) is also one of the CL derivatives. It is synthesized by the sulfotransferase family 2B member 1 (SULT2B1) (13) and is a component of the cell membrane, especially in the plasma human blood layer (14,15). Additionally, there are reports that CS is important for developing skin cells (16), the acquisition of sperm fertilization (17,18), and the prevention of blood clotting (19). Moreover, CS's ability to modify the physical properties of the membrane also influences the stabilization and inhibits the fusion of membranes (14,15,20,21).

Despite the essential roles of CS in many physiologic and pathophysiologic conditions, the function of CS on the immune system remains largely unknown. For example, Wang et al. (22) reported that excessive CS inhibits TCR signaling by interfering with TCR nanocluster formation and avidity. However, it was unclear how CS affected TCR clustering before TCR stimulation. In addition, whether CS controls the quantitative changes and dynamics of TCR on the T cell membrane also remains unknown. Nevertheless, several recent studies have demonstrated that specific cell membrane structures or areas could play a key role in certain immune responses. Interestingly, the microvilli, protrusive cell membrane structures mainly composed of actin filaments, are concentrated with such important T cell molecules as TCRs and TCR complexes and serve as docking platforms for T cells to recognize Ags during T-cell interactions with cognate Ag-presenting cells (APCs) (23-25).

Therefore, this study investigated whether CS could alter T-cell-mediated immunity *in vitro* and *in vivo* using electron microscopy. Next, we carefully observed whether CS affects the membrane structure of T cells. Remarkably, although CS dramatically distorted the structure of microvilli and significantly reduced surface microvilli-associated proteins, it did not induce cell death. We also observed that CS interacts competitively with the cell membrane with CL, releasing microvilli, which results in attenuated TCR signaling and weakened T cell adhesion on cognate APCs. Based on these findings, we further investigated its effect in autoimmune disease models, and CS showed an immunosuppressive therapeutic potential by inhibiting T cell homing and activation.

MATERIALS AND METHODS

Abs and reagents
Abs for TCRα (ab18861), CD3ζ (ab135372), LAMP-1 (ab24170), Rab11 (ab3539), and PMCA ATPase (ab2825) were purchased from Abcam (Cambridge, MA, USA). Abs against CD3ζ and CXCR4 were purchased from Santa Cruz Biotechnology (Dallas, TX, USA). Abs against CD3ζ (cst88083), ZAP70 (cst2075), phospho-ZAP70 (cst2717), LCK(cst2752), phospho-LCK (cst2751), Erk1/2 (cst4695), phospho-Erk1/2 (cst4396), p38 (cst8690), phospho-p38 (cst9215), Akt (cst4691), phospho-Akt (cst4060), PKCθ (cst9616), phopho-PKCθ (cst9376), β-actin (cst8457), anti-rabbit IgG-HRP (cst7074), and anti-mouse IgG-HRP (cst7076) were purchased from Cell Signaling Technology (Danvers, MA, USA). Fluorescence-conjugated

anti-TCRβ (109212), CD62L (104412), CD45 (368512), CD3ζ (152304), CD44 (103007), and ZAP70 (313404) were purchased from BioLegend (San Diego, CA, USA). Anti-TCRβ (H57-597) was purchased from Bio-X-Cell (West Lebanon, NH, USA). TRITC-labeling kit, CellTracker™ Green CMFDA, Orange CMRA, Deep Red dyes, CellTrace™ Violet, and Annexin V-PE Conjugate, Propidium Iodide, Cholera Toxin Subunit B (Recombinant), Alexa Fluor™ 594 Conjugate, and Fab preparation kit were purchased from Thermo Fisher Scientific (Waltham, MA, USA). Recombinant mouse ICAM-1, mouse IL-2 DuoSet ELISA, mouse IFNγ DuoSet ELISA, and Substrate Reagent Pack (DY999) were purchased from R&D Systems (Minneapolis, MN, USA). Poly-L-lysine (PLL) (A-005-C), phorbol 12-myristate 13-acetate (PMA) (79346), filipin (F4767), 50% glutaraldehyde (340855), 3,3′-Diaminobenzidine (D8001), and osmium tetroxide (O5500), Sodium cholesteryl sulfate (C9523), CL (C3045), ionomycin (IO, I0634), and 2-Chloro-2,4,6-trinitrochlorobenzene (TNCB) (79874) were purchased from Merck (Darmstadt, Germany). House dust mite extract was purchased from Creative Biomart (Shirley, NY, USA). MHC I-A^b was provided by the NIH Tetramer Core Facility (Atlanta, GA, USA). WEST-ZOL (16021) western blot detection kit was purchased from Intron Biotechnology (Seongnam, Korea). Complete protease inhibitors and phosphatase inhibitors were purchased from Roche Applied Science (Indianapolis, IN, USA). Ovalbumin (OVA) peptide fragments (323–339 and 257–264) were purchased from GeneScript (San Francisco, CA, USA). Electron microscope reagent for LR white resin, uranyless, and copper gird were purchased from Electron Microscopy Sciences (Hatfield, PA, USA).

Cells

Naïve CD3$^+$ T cells were isolated from the mouse (C57BL/6 or BALB/c) spleen and lymph nodes (LNs) by negative selection using a MojoSort™ Mouse CD3 Selection Kit (BioLegend, San Diego, CA, USA). To generate mouse T cell blasts, CD3$^+$ T cells were stimulated on 2 μg/ml α-CD3/28-coated culture plates with 100 U/ml rIL-2 for 48 h and cultured for 5 days with 100 U/ml rIL-2. All mouse T cells were incubated in mouse T cells media. Naïve B cells were isolated from the spleen using EasySep™ Mouse B Cell Isolation Kit (Stemcell Technologies, Vancouver, Canada). To generate mouse B cell blasts, CD19$^+$ cells were cultured for 3 days in complete RPMI containing LPS (10 μg/ml). The purity of each population was confirmed as >95% by flow cytometry. For the isolation of bone marrow-derived dendritic cells (BMDCs), bone marrow was flushed from the femur and tibia bones, 5×10^6 cells were cultured in 10 ml of RPMI 1640 medium supplemented with 20 ng/ml recombinant murine granulocyte-macrophage colony-stimulating factor (GM-CSF) for 9 days. GM-CSF was added at every 3 days.

Animals

C57BL/6 wild-type, BALB/c, *OTI*, and *OTII* TCR transgenic mice (C57BL/6 background) were purchased from the Jackson Laboratory (Bar Harbor, ME, USA). All mice were housed in specific pathogen-free conditions. All experimental methods and protocols were approved by the Institutional Animal Care and Use Committee of the School of Life Sciences, Gwangju Institute of Science and Technology, and performed in accordance with their approved guidelines. In general, sex-matched, 8-week-old mice were used.

CL and CS treatment *in vitro* and *in vivo* and T cell stimulation

CD3$^+$ T blasts were treated with either CL (100 μM) or CS at various concentrations (1–500 μM) for 3 h. EtOH (0.2%) or DMSO (0.1%) were used as a vehicle control, respectively. For systemic treatment, recipient mice were given 100 or 200 μM of CS 3 times every 8 h and sacrificed after 24 h from the last infection. In some experiments, CD3$^+$ T blasts were pre-incubated in 50 mM methyl-β-cyclodextrin (MβCD) for 30 min. For T cell stimulation, CD3$^+$

T blasts were treated as described above, washed with PBS, and stimulated with plate-bound anti-CD3/28 Abs or PMA/IO for 24 h. In some experiments, OTII CD4$^+$ or OTI CD8$^+$ T cells were treated as described above and activated by coincubation with pOVA$_{323-339}$ or $_{257-264}$-pulsed dendritic cells (DCs) for 24 h and the supernatants were subjected to ELISA assay to examine cytokine production.

Western blot

Cells were lysed in ice-cold lysis buffer (50 mM Tris-HCl pH 7.4, 150 mM NaCl, 1% Triton X-100, 1× complete protease/phosphatase inhibitor cocktail) for 1 h on ice. Lysates were centrifuged at 16,000 ×g for 25 min at 4°C and the protein concentration was determined according to Bradford. An equal amount of protein in each samples (10–20 μg) were mixed with SDS sample buffer (100 mM Tris-HCl pH 6.8, 4% SDS, 20% glycerol, bromophenol blue), heated for 5 min, separated with 10%–12% SDS-PAGE, and transferred to nitrocellulose membranes using a Trans-Blot SD Semi-Dry transfer cell (Bio-Rad, Hercules, CA, USA). Membranes were then blocked in 5% skim milk for 1 h, rinsed, and incubated with primary Abs in TBS containing 0.1% Tween 20 (TBS-T) and 3% milk overnight. Excess primary Ab was removed by washing the membrane four times in TBS-T before incubation with peroxidase-labeled secondary Ab (0.1 μg/ml) for 1.5 h. Bands were visualized with a WEST-ZOL Western Blot Detection kit and exposed to X-ray film.

Flow cytometry

CD3$^+$ T blasts were treated with CL (100 μM), CS (100 μM), or vehicle for 3 h, washed with PBS, and stained with florescence-conjugated Abs for 1 h at 4°C or 37°C. For intracellular staining, cells were permeabilized using Cytofix/Cytoperm (Invitrogen, Carlsbad, CA, USA) and stained with the indicated Ab for 1 h at 4°C. Cells were then washed with PBS and melt flow index was determined by FACS Canto (BD Biosciences, San Jose, CA, USA) and analyzed with FlowJo software (Tree Star, Inc., San Carlos, CA, USA).

Conjugation assay

OTII CD4$^+$ T cells were treated as described above and stained with Cell Tracker Green CMFDA. CD19$^+$ B blasts were stained with Cell Tracker Orange CMRA for 30 min. Cells were then washed and resuspended in RPMI 1640 media. For conjugation, B cells were incubated with T cells (1:1 ratio) for 1 h in the presence or absence of pOVA (323–339, 1 μg/ml). The relative proportion of green, orange, and green and orange-positive events in each tube was determined by flow cytometry. The number of gated events counted per sample was at least 30,000. The percentage of conjugated T cells was determined as the number of dual-labeled (green and orange-positive) events divided by the number of green-positive T cells.

TIRF microscopy

The planar lipid bilayer was prepared as previously described (24). OTII CD4$^+$ T cells were treated with CS (100 μM) or vehicle and stained with TRITC-labeled anti-TCRβ Fab for 1 h at 4°C. Cells were then washed with cold PBS 3 times and resuspended with HEPES imaging buffer. The cells were placed on a planar lipid bilayer presenting OVA$_{323-339}$-I-A^b/ICAM-1 and were immediately imaged for 20 min using TIRF microscopy (IX-81; Olympus, Tokyo, Japan) equipped with a solid-state laser (543 nm, 20 mW; Coherent, Santa Clara, CA, USA). TCRβ centripetal movements and kymograph were tracked using Image J software.

Confocal microscopy

CD3+ T blasts were treated with CL (100 μM), CS (100 μM), or vehicle for 3 h and cells were rinsed three times with PBS. Cells were stained with TCRβ-Fab-TRITC for 1 h at 4℃ or 37℃. TCRβ internalization was observed by using a 100× NA 1.40 oil immersion objective and an FV1000 laser scanning confocal microscope (Olympus). To determine the influence of CL or CS in lipid raft distribution, cells in each condition were stained with cholera toxin subunit B (CTB)-Alexa594 for 30 min at 37℃. To measure the CL level in the cell membrane, cells in each condition were fixed with 4% paraformaldehyde for 30 min and stained with filipin (50 μg/ml) for 2 h at room temperature (RT). Cells were rinsed with PBS three times and the images were obtained using 405 nm solid-state lasers of Zeiss LSM 880 confocal laser scanning microscope (Carl Zeiss, Oberkochen, Germany). Intensity histogram of CTB and filipin were calculated automatically by ZEN software.

Two photon imaging

To analyze T cell homing in vivo, naïve CD3+ T cells isolated from C57BL/6 mice were treated with CS (100 μM) or vehicle as described above and stained with CMFDA or CMRA for 30 min at 37℃, respectively. Recipient C57BL/6 mice were anesthetized by intraperitoneal injection of 1.2% avertin (2,2,2-tribromoethanol dissolved in 2-methyl-2-butanol), and the popliteal LN was exposed by small skin incisions and bathed with a continuous flow of warm saline to maintain a local temperature at 37℃ during the imaging. The labeled cells were mixed at a 1:1 ratio in 200 μl of dextran, Cascade Blue™ and adoptively transferred to recipient mice intravenously (i.v.). Cells on high endothelial venule (HEV) were immediately imaged for 2 h using Zeiss LSM 880 microscope equipped with a MaiTai laser (Coherent) tuned to 780 nm in combination with an NDD2 BIG2 GaAsP detector and a 20× water-dipping lens (NA 1.0; Carl Zeiss) using ZEN v2.1 acquisition software. For analyze DC-T cell interactions *in vivo*, pOVA (323–339, 1 μg/ml)-pulsed BMDCs (5×10^6) were stained with Cell Tracker CMRA-orange and injected subcutaneously (s.c.) into the footpads of recipient mice. At 24 h post injection, CS or vehicle treated OTII CD4+ T cells were stained with CMFDA-green and adoptively transferred to recipient mice i.v. with 200 μl of dextran, Cascade Blue™. The number of T cells, DCs, and conjugation ratio DC-contacted T cells, speed, displacement, and duration of interactions were analyzed using Imaris software. Data were plotted using Prism (GraphPad, San Diego, CA, USA).

Quantification of 2 photon images

In 3 independent experiments, all fluorescence-labeled T cells were detected using the Imaris 8.0 software. Migration (%) of splenocytes and lymphocytes was determined as the number of CMFDA+ (CS-treated)/CMRA+ (DMSO-treated) ×100% in a sectioned area (4 mm^2). The entry of T cells into splenic T-zone (%) was determined as the number of CMRA+ (DMSO-treated) or CMFDA+ (CS-treated) in T-zones /total number of CMRA+ and CMFDA+ in the sectioned area (4 mm^2) ×100%. The number of adherent cells on HEV was determined by T cells with a duration time of 3,000 s or more among T cells located on HEV. The duration time, displacement length, speed, and trace of migrated T cells into HEV were analyzed in obtained 2-photon data movies (n=3) using Imaris 8.0 software.

ELISA

Mouse serum was obtained from the orbital vein of atopic dermatitis (AD) induced mice. The amounts of IL-2 and IFN-γ in the serum for each condition were determined by ELISA with Duo Set Mouse ELISA kits for IL-2 and IFN-γ (R&D Systems) according to the manufacturer's instructions.

Immunocytochemistry

Naïve CD3$^+$ T cells were treated with CS (100 μM) or vehicle as described above and stained with CMFDA or CMRA for 30 min at 37℃, respectively. The labeled cells were mixed at a 1:1 ratio in 200 μl of PBS and adoptively transferred to recipient mice i.v. Spleen and popliteal LNs were harvested at 2 h post-injection and fixed in 4% paraformaldehyde in PBS at 4℃ overnight. On the next day, the samples were washed and incubated in PBS with 30% sucrose (w/v) (Sigma-Aldrich, St. Louis, MO, USA) overnight at 4℃. The samples were then embedded in Tissue-Tek® O.C.T. Compound (Thermo Fisher Scientific) and frozen using 2-methylbutane, cooled with liquid nitrogen. 10 μm sections were cut using a Leica CM1800 cryostat. For immunostaining, tissue sections were blocked for 2 h in 10% normal goat serum at RT. The sections were incubated with fluorescently conjugated anti-B220 Ab at RT for 30 min in 10% goat normal serum. The samples were washed three times to remove unbound Ab and mounted in Permount solution (Thermo Fisher Scientific). Images were acquired with a confocal microscope and analyzed with FluoView software (Olympus). The epidermal/dermal depths and CD3ζ-3,3'-diaminobenzidine (DAB)$^+$ cells were measured on 12 slides from 6 mice using EVOS FL Auto 2 software (Invitrogen).

Microvilli particles isolation

CD3$^+$ T blasts were treated with either CS (100 μM) or vehicle for 3 h. Cells and media were harvested, centrifuged at 2,000 ×g for 10 min 3 times to remove cells and debris. Supernatants were further subjected to ultracentrifugation at 100,000 ×g for 1 h at 4℃. Microvilli particles were used for western blot, scanning electron microscopy, or transmission electron microscopy (TEM) imaging.

Electron microscopy

To prepare the scanning electron microscopy samples, 0.1% DMSO, CL (100 μM), MβCD (50 mM), CS (100 μM)-treated T blasts were incubated on the PLL-coated silica plate for 30 min and fixed by using 2.5% glutaraldehyde in 0.1 M sodium cacodylate for overnight at 4℃. The samples were rinsed three times with 0.1 M sodium cacodylate and incubated with 30%, 50%, 70%, 90%, and 100% EtOH in concentration order for 10 min. after being rinsed with 100% EtOH 2 times for 10 min, the samples were put in hexamethyldisilazane for 5 min. Then, those were dried at RT for 24 h and imaged using scanning electron microscopy. To establish the TEM samples the T blasts were incubated on the PLL-coated 18 mm circular cover glass on the culture plate and put in mouse T cell media containing 0.1% DMSO or CS (100 μM) for 3 h. after being washed with PBS 3 times, the cells on the cover glass were incubated with Karnovsky's solution (2% paraformaldehyde and 2.5% glutaraldehyde in 0.1 M cacodylate buffer) for 24 h at 4℃. After that, the cells were post-fixed with 1% osmium tetroxide for 1 h and washed with 0.1 M cacodylate buffer three times. The fixed cells were dehydrated with 50%, 70%, 90%, 100%, for 10 min and embedded with 1:1 EtOH:resin (for overnight) and 100% Resin (for 2 h) on a rotator. BEEM® capsule filled with resin was placed on a cover glass and left for 24 h without oxygen for resin polymerization. After the cover glasses present on the surface were removed using liquid nitrogen, the resin capsules including the sample were sectioned to 70 nm using an ultramicrotome (Leica EM UC6; Leica, Wetzlar, Germany). Resin sections were placed on a grid and stained by Uranyless for 1 min. Images were obtained using Tecnai G2 electron microscope (FEI, Hillsboro, OR, USA) at 120 kV under low-dose conditions. To analyze the number of T cell microvilli imaged by scanning electron microscopy, the number of microvilli/2D outline of the cell was calculated automatically using Filopodyan ver.1.3.1. The filopodyan details have been adjusted to Treshhold= triangle, ED Iteration = 8, Base Back Frames= -3, LoG sigma= 3.

RT-PCR and real-time quantitative PCR (qPCR)

CD4$^+$ T cells (5×10^6) were cultured with 100 μM CS for 3 h and RNA was extracted from the cultured cells with TRI reagent (Molecular Research Center, Cincinnati, OH, USA). After then, we performed reverse-transcribed with RT-Premix (DN6; Enzynomics, Daejeon, Korea) and performed real-time qPCR with the below primer sequences(the forward and reverse pairs are written): mouse TCRα 5′-CATCCAGAACCCAGAACCTGC-3′ and 5′-GGGAGTCAAAGTCGGTGAACA-3′; and mouse CD3ζ, 5′-GCTCCAGGATTTCTCGGAAGTC-3′, and 5′-ATGGCTACTGCTGTCAGGTCCA-3′; and mouse CD44, 5′-CCTTGGCCACCACTCCTAAT-3′ and 5′-ATGGTTGTTGTGGGCCGAA -3′; and mouse L-selectin, 5′-GACATGGGTGGGAACCAACA-3′, and 5′-CACTGGACCACTGTGTAGCA-3′. Amplification was performed in a StepOne real-time PCR system (Applied Biosystems, Norwalk, CT, USA) for continuous fluorescence detection in a total volume of 10 μL of cDNA/control and gene-specific primers using SYBR Premix Ex Taq (TaKaRa Bio). The mRNA levels of the target genes were normalized relative to those of Gapdh using the following formula: relative mRNA expression = 2−(ΔCt of target gene − ΔCt of GAPDH), where Ct is the threshold cycle value. In each sample, the expression of the analyzed gene was normalized to that of Gapdh.

Induction of AD

Briefly, sex-matched and 8-week-old wild-type BALB/c mice were used for AD induction. Six mice were used in each group for AD induction experiments. The surfaces of both ear lobes were stripped five times with surgical tape before being treated with TNCB and mite solution to remove dead skin cells and scabs on the ear surface. TNCB was dissolved in the 3:1 mixture of acetone and olive oil. To establish TNCB sensitization in BALB/c mice ears, 200 μl of 1% TNCB was applied onto each ear (day −7). At day 0, 200 μl of 0.2% TNCB was applied onto each ear again, followed by 20 μl of house dust mite extract (10 mg/ml) on day 4. Thereafter, TNCB and mite extract were applied alternately at 3–4 days intervals for 3 weeks. Simultaneously, mice received the 200 μl PBS containing 0, 10, and 25 μg of CS i.v. at 3-day intervals from day 0. Ear thickness was measured using calipers on days −7, 1, 4, 8, 11, 15, 18, and 21. The ear tissue was excised in each group and subjected to histopathological analysis. Spleen and draining LN were isolated from 6 AD-induced mice on day 21 and measured the size and volume using caliper (n=6). CD3$^+$ T cells were then isolated, stimulated on an α-CD3/28 coated plate for 8 h, and CD69/25 was measured by flow cytometry. For adoptive transfer experiment, CD3$^+$ T cells were isolated from each group of mice at day 21 following AD induction and adoptively transferred to a new set of recipient mice at a dose of 5×10^6 cells. Subsequently, mice were also subjected to the challenging with TNCB and mite for 7 days.

Immunohistochemistry (IHC)

Ears from each group were fixed in 10% paraformaldehyde and embedded in paraffin. Paraffin blocks were sliced into 10 μm-thick sections, deparaffinized, and stained with H&E. The thickness of the epidermis and dermis on the sections was measured. To analyze infiltrating T cells in the ear tissues, sections were blocked with 2% rat serum in PBS and incubated with primary CD3ζ Ab (ab135372) for overnight at 4℃. Sections were rinsed with PBS 3 times, incubated with secondary Ab for 1 h at RT, and DAB was dropped in the tissue sections for 10 min. IHC images were acquired using EVOS FL Auto 2 (Invitrogen).

Statistics

Student's *t*-test and one-way ANOVA analysis of variance (corrected for all pairwise comparisons) were performed using Prism software. $p < 0.05$ was considered statistically significant.

RESULTS

CS inhibits T-cell activation mediated via TCR signaling

It has been shown that the excessive exposure of CS to T cells inhibits TCR signaling and disrupts TCR-nanoclusters (22). This finding led us to determine how CS affects TCR signaling and TCR nanoclusters. First, we investigated whether external treatment with CS could inhibit TCR-stimulated T cell activation as a first approach. With a notable difference in the external CS concentration (up to 100 μM) (**Fig. 1A**), IL-2 cytokine release was significantly, and CS dose-dependently reduced in T cells placed on immobilized anti-CD3/CD28 Abs (**Fig. 1A**). Although the effect of CS was time-dependent at 100 μM CS, this concentration had little effect on PMA/IO-induced T cell activation, suggesting that CS only affects signaling through TCR (**Fig. 1B**). However, CL itself had little effect on T cell activation induced by immobilized anti-CD3/CD28 Abs (**Fig. 1A**).

Subsequently, we applied the CS to OTI and OTII mouse T cells activated on DCs pulsed with OVA-peptides to confirm the physiologic significance. Similar to plate-coated α-CD3/CD28-Abs stimulation, these T cells significantly reduced cytokines IL-2 and IFN-γ (**Fig. 1C**). In addition, CS also significantly inhibited T-cell spreading during activation (**Fig. 1D**). Our results further established that the attenuation of T cell activation by CS was not due to CS-induced apoptosis (**Fig. 1E**). Taken together, we corroborated that CS could cause defects in TCR-mediated signaling, thereby attenuating T cell activation.

CS independently depletes surface proteins related to T cell activation before internalization

Attenuated TCR signal strengths may be due to a decrease in surface TCR molecules or, otherwise, a blocking of internal signaling pathways (26,27). We, therefore, compared the expression of various surface proteins, including those of the TCR and CD3 complexes, after T cells were treated with CS. Flow cytometric analysis showed that T cells exposed to CS had lower TCR and CD3 complex expression than that of nontreated T cells (NT) (**Fig. 2A**). Given that recent reports demonstrated that the TCR and CD3 complexes are localized at the tips of microvilli of T cells (23,24), we subsequently determined whether other microvilli-specific proteins were also decreased. Interestingly, lower L-selectin and CD44 protein expression was observed. Besides, the expression of CD45, which was evenly present in the cell membrane, was not changed (**Fig. 2A**). To examine whether CS affect mRNA expression of those proteins, we examined mRNA levels of microvilli-localized proteins treated with either DMSO or CS for 3 h. Unexpectedly, we found that mRNA expression of *TCRα*, *CD3ζ*, *CD62L*, and *CD44* was also slightly affected by CS treatment (**Fig. 2B**). However, the mRNA level of *CD45* was not affected, which is consistent with the unaltered expression of CD45 protein on the surface of the cell. To address whether the decrease in surface protein caused by CS is a result of altered mRNA expression, we treated cells with CS for only 1 h, using the same concentration. Interestingly, the treatment of CS at a concentration of 100 μM also led to a significant decrease in the expression of the microvilli-specific protein on the surface, without a corresponding decrease in mRNA expression (**Supplementary Fig. 1**), suggesting that the reduction in protein expression on the cell surface at 3 h was not caused by a decrease of mRNA expression. Accordingly, we observed that CS reduced the number of TCR microclusters and dramatically inhibited their movement toward central-supramolecular activation clusters (c-SMAC) (**Fig. 2C**, **Supplementary Video 1**). It has also been well documented that a decrease in TCR expression on the T cell surface after activation is associated with TCR internalization (28). Thus, we further confirmed whether the decrease
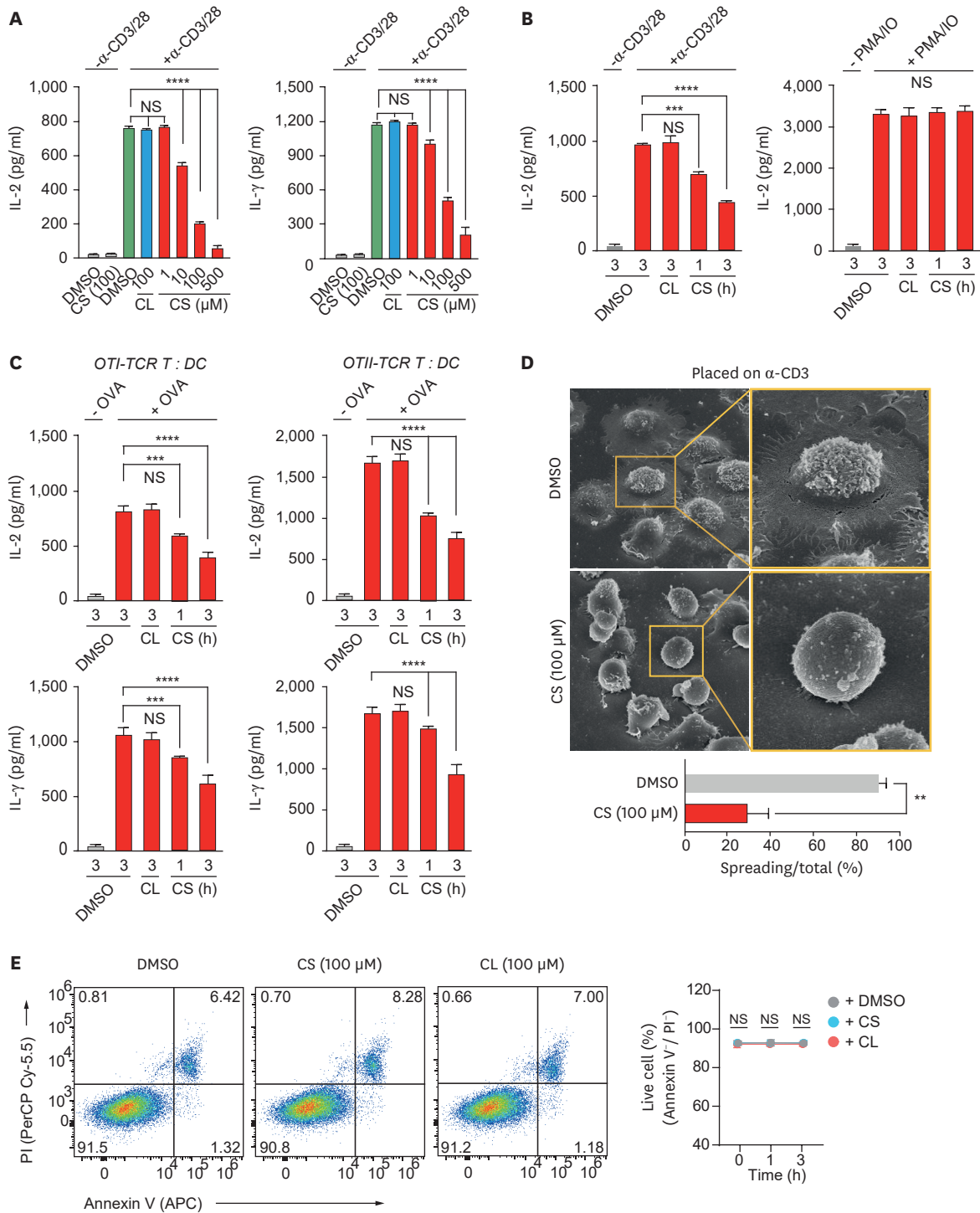
Figure 1. Attenuated immune response to excessive CS.

(A) CD3^{+} T blasts dose-dependently treated with a vehicle, CL (100 μM), or CS (1–500 μM) for 3 h, and then stimulated on α-CD3/28-coated plate for 24 h. Subsequently, ELISA measured the levels of secreted IL-2 or IFN. All results are representative of three independent experiments. (B, C) T cells from wild-type (CD3^{+}), OTI (CD8^{+}), or OTII (CD4^{+}) mice treated with a vehicle, CL, or CS (100 μM each) for the indicated periods, and then they were stimulated by a α-CD3/28 Abs coated plate, PMA/IO treatment, or co-cultured with pOVA-loaded DCs for 24 h. Subsequently, ELISA measured the levels of secreted IL-2 or IFN. (D) CD3^{+} T blasts treated with a vehicle or CS (100 μM) and placed on α-CD3/28-coated plates for 5 min. An initial spreading of T cells was observed through scanning electron microscopy (n=40). (E) Determination of the toxicity of CS or CL. CD3^{+} T blasts were treated with a vehicle, CS, or CL (100 μM each) for the indicated periods. Then, apoptotic cells were analyzed by flow cytometry using annexin V-propidium iodide staining. All results are representative of three independent experiments. Data are presented as mean ± SEM.
**p<0.01, ***p<0.001, ****p<0.0001.

in TCRs by CS was related to TCR internalization. To this end, we stained CD3⁺ T cells with a Cy5-conjugated anti-TCRβ Fab Ab at 4°C and 37°C. Then, the cells were cultured in media containing CS for 3 h, after which we measured the localization and TCRβ expression. DMSO- and CL-treated groups showed the same TCR expression, regardless of TCR internalization. In contrast, CS-treated T cells had a low TCR expression in both conditions with and without internalization (**Fig. 2D**). The results thus far demonstrate that CS may reduce surface T-cell proteins by releasing or collapsing outside the membrane rather than after internalization.

CS reduces lipid raft's composition on T-cell surfaces

CS is biosynthesized by replacing the −OH CL residue with a sulfate group, using the enzyme SULT2B1, which leaves the other groups unchanged ([13]). However, it is still unclear whether there is any difference in T cells exposed between CS- and CL-excessive milieu. It has also been reported that both CS and CL are closely related to the cell membrane compositions ([1],[14],[20],[21]). For example, CL is enriched in lipid rafts ([4]). Therefore, we investigated whether CS- and CL-excessive environments can change the lipid raft composition. The CTB, a ganglioside GM1 maker, was used to detect the lipid raft level on the membrane. Investigations revealed that the CTB expression showed no difference in CL-treated T cells compared with DMSO-treated cells (**Supplementary Fig. 2A**). However, the CTB binding was significantly decreased in T cell membranes treated with CS.

Subsequently, we used a specific CL tracker, filipin, to determine membrane CL levels. When T cells were treated with CS, CL levels on the cell membrane were dramatically reduced (**Supplementary Fig. 2B**). However, with CL treatment, extreme CL conditions resulted in increased intracellular CL levels, presumably through receptor endocytosis (**Supplementary Fig. 2B**). Furthermore, treatment with MβCD, a CL chelator, almost completely reduced CL levels on the T cell membrane as expected (**Supplementary Fig. 2B**).

Excessive CS releases T-cell microvilli, resulting in T cell dysfunction

It was interesting that CS inhibited lipid rafts by depleting some surface proteins. This finding suggests that CS can quickly disrupt particular areas on the cell membrane (**Fig. 3A**). Previous studies have demonstrated that although lipid rafts are abundant in microvilli, the depletion of sphingolipids or CL inhibits microvilli formation ([29-31]). Coincidently, the TCR-CD3 complex, including CD28, CXCR4, and CD44, are abundant in T-cell microvilli ([23],[24]). These findings suggest that CS can change the shape of T-cell microvilli. In this study, using an electron microscope, we observed the shapes and numbers of T-cell microvilli under various treatment conditions (CS, CL, and MβCD) (**Fig. 3A**, **Supplementary Fig. 3**). Investigations revealed that the number of microvilli was substantially reduced in T cells treated with MβCD (**Fig. 3A**). Interestingly, the treatment with external CS also decreased the number of T-cell microvilli (**Fig. 3A**). Moreover, while external CL did not recover the loss of microvilli by CS, the loss by MβCD was recovered by external CL (**Fig. 3A**), suggesting that the action mechanism of CS was different from that of MβCD. Additionally, given that both CS and CL are structurally similar groups, they may share similar regions in the lipid rafts. As a result, both CS and CL competitively deformed and formed the microvilli (**Fig. 3A**). We also observed that CS-treated T cells fully, dose-dependently, and time-dependently recovered the microvilli 24 h after replacement with fresh culture media (**Fig. 3B**, **Supplementary Fig. 4**).

Subsequently, we carefully observed T cells through scanning electron microscopy and TEM to determine how surface microvilli disappear when T cells are treated with CS. Surprisingly,
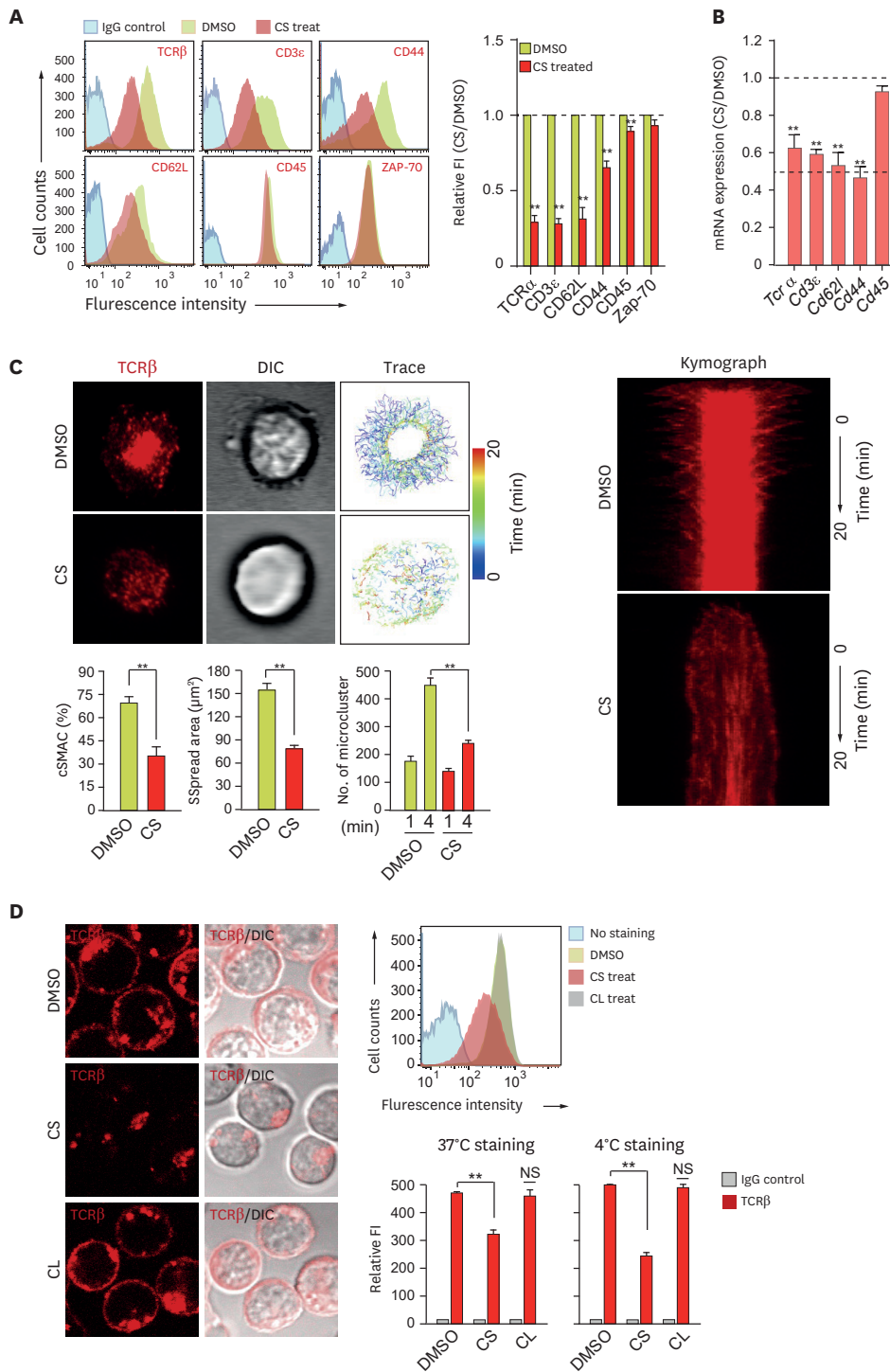
Figure 2. External CS suppresses the immune synapse formation by reducing the number of TCRs.
(A) CD3^{+} T blasts were treated with a vehicle or CS (100 μM) for 3 h, stained with indicated Abs against the proteins potentially enriched or excluded from microvilli, and analyzed by flow cytometry. (B) Cells treated as (A) for 3 h were lysed and mRNA expression of the indicated genes were measured by RT-qPCR. (C) OTII CD4^{+} T cells treated as (A), and then stained with anti-TCRβ (H57Fab-Alexa594), followed by a planar bilayer examination, presenting OVA-$_{323-339}$/I-A^b and ICAM-1. Representative images of c-SMAC formation, the trajectory of individual TCR-microclusters, and a kymograph are presented. All images were analyzed using the Imaris 8.0 software, after which statistical analysis results were presented. All results are representative of three independent experiments (n=10). (D) CD3^{+} T blasts stained with anti-TCRβ (H57Fab-Alexa594) for 1 h at 37℃ or 4℃, then washed with PBS. Subsequently, cells were treated with CS or CL for 3 h, followed by observing the TCRβ distribution under a confocal microscope. All results are representative of 3 independent experiments.
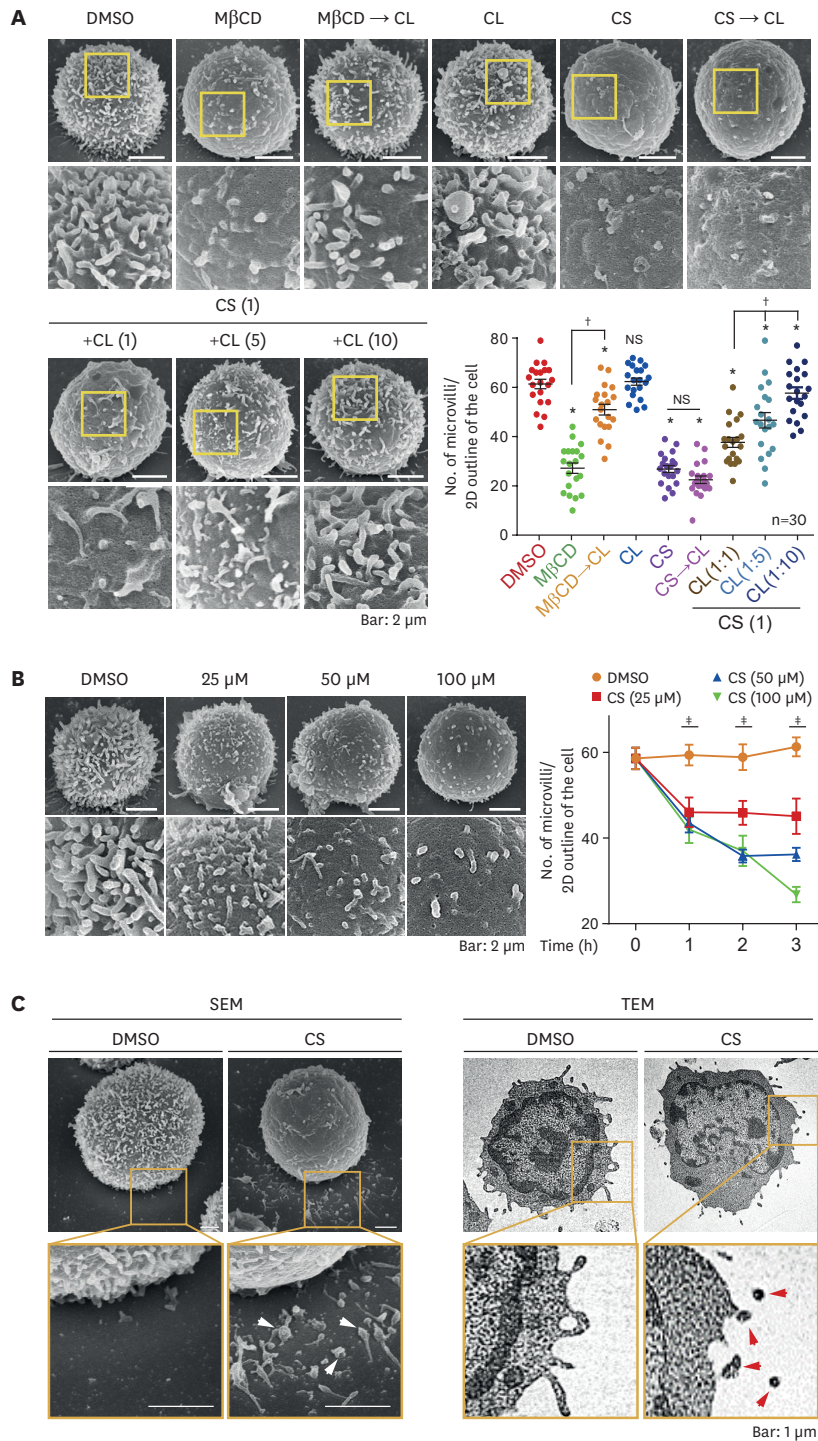Data are presented as mean ± SEM.
**p<0.01.

Figure 3. Excessive CS exposure causes the depletion of microvilli in the T cells.
(A) Scanning electron microscopy images showing microvilli on T cell surfaces in a CS-excessive environment. CD3^{+} T blasts were treated with 100 µM CS, 100 µM CL, or vehicles for 3 h at 37 °C. Then, T cells were pre-treated with 50 mM MβCD for 30 min for MβCD treatment. In some experiments, cells were simultaneously treated with CS and CL at 1:1 to 1:10 ratios (1:100 µM; 5:500 µM; 10:1,000 µM). Finally, the number of microvilli/2D outlines of the cell for (A) and (B) were analyzed using ImageJ software-Filopodyan. *p<0.01 vs. DMSO, †p<0.01 (n=30). (B) Scanning electron microscopy images showing microvilli on dose and time-dependent CS-treated T cell surfaces. ‡P<0.01 vs. DMSO (0 h). (C) Scanning electron microscopy and TEM images showing microvilli shedding in CS-treated cells. CD3^{+} T blasts were placed on a PLL-coated silica plate for 30 min, and then treated with 100 µM CS for 3 h. Then, the cells were fixed and observed through scanning electron microscopy and TEM. White and red arrows represent shed microvilli particles from T cells.
Data are presented as mean ±SEM.

the treatment of T cells with CS remarkably released microvilli particles from the bottom area (**Fig. 3C**). Therefore, these results demonstrate that external CS could competitively induce the loss of surface microvilli in T cells in the presence of extracellular CL.

The sizes of microvilli-derived particles were lower than 200 nm (**Fig. 4A**) and comparable with the microvesicles being released within T cells ([32](#)). Based on this finding, we collected the microvilli-derived particles from CS-treated T cells to determine which proteins were enriched in these particles. Western blotting revealed that the particles contained higher microvilli proteins such as TCR, CD3s, CXCR4, and LCK than that of the total cell lysates (**Fig. 4A**). In contrast, markers for macrovesicles such as LAMP-1 or Rab11 were almost absent, suggesting that the particles released by CS were derived from T-cell microvilli (**Fig. 4A**).

Although some reports have implied the importance of the morphology or function of the T cell microvilli ([23-25](#)), the physiological relevance of microvilli defects in T cells is largely unknown. Thus, we hypothesized that microvilli loss by CS may induce significant T-cell-mediated immune response defects. Investigations revealed that OTII T cells treated with CS significantly reduced the binding capacity to OVA-pulsed APCs (**Fig. 4B**). Moreover, when T cells were activated using immobilized α-CD3/28 Abs, CS-treated T cells markedly reduced the downstream phosphorylation of signaling proteins in TCRs (**Fig. 4C**). Contrastively, the phosphorylation levels were affected when CS-treated T cells were stimulated with PMA/IO (**Fig. 4C**), suggesting that TCR-independent signaling molecules are intact in CS-treated T cells.

CS has an immunosuppressive potential and can be applied to hyper-immune treatments

Given that CS effectively reduces T cell responses by affecting microvilli-associated TCR signaling, we further examined whether CS suppresses T-cell-mediated immunological diseases such as AD. To investigate the influence of CS to T cells *in vivo*, CS was i.v. injected into recipient mice for 24 h to foster the circulation of CS in the blood. CD3$^+$ T cells were then isolated, CD69 and CD25 expression were determined as activation markers. Flow cytometric analysis revealed that T cells obtained from CS-injected mice had reduced expression of CD69 and CD25 in response to the anti-CD3/CD28 Abs but not PMA/IO (**Fig. 5A**). This finding is consistent with the *in vitro* effect of CS on T cells presented in **Fig. 1A-C**.

Subsequently, to examine the effect of CS *in vivo*, we induced AD in the ears of mice (**Supplementary Fig. 5**). Certain concentrations (10–25 μg) of CS were injected i.v. at 3 days interval. Three weeks later, macroscopic and microscopic assessments were conducted. Investigations revealed that mice injected with CS had dramatically alleviated AD compared with that in the PBS-injected mice (**Fig. 5B and C**). Furthermore, the number of infiltrating T cells (CD3ζ) in the ear tissue also diminished in mice injected with CS (**Fig. 5D**). Moreover, while there were more volumes of spleen and LNs in the CS group than in the MOCK group, the reduced expression of CD69 and CD25 in the T cells isolated from the CS-injected groups manifested attenuated immune responses (**Fig. 5E and F**).

To confirm the alleviated AD symptom in CS-injected mice is mediated by T cells, we induced AD in mice for 21 days as presented in **Supplementary Fig. 5**. The CD3$^+$ T cells purified from PBS or CS-injected mice at day 21 were adoptively transferred into wild-type recipients, that were challenged with TNCB and mite after transfer (**Fig. 6A**). Mice adoptively transferred with CD3$^+$ T cells isolated from PBS-injected mice developed a severe skin inflammation at day 7
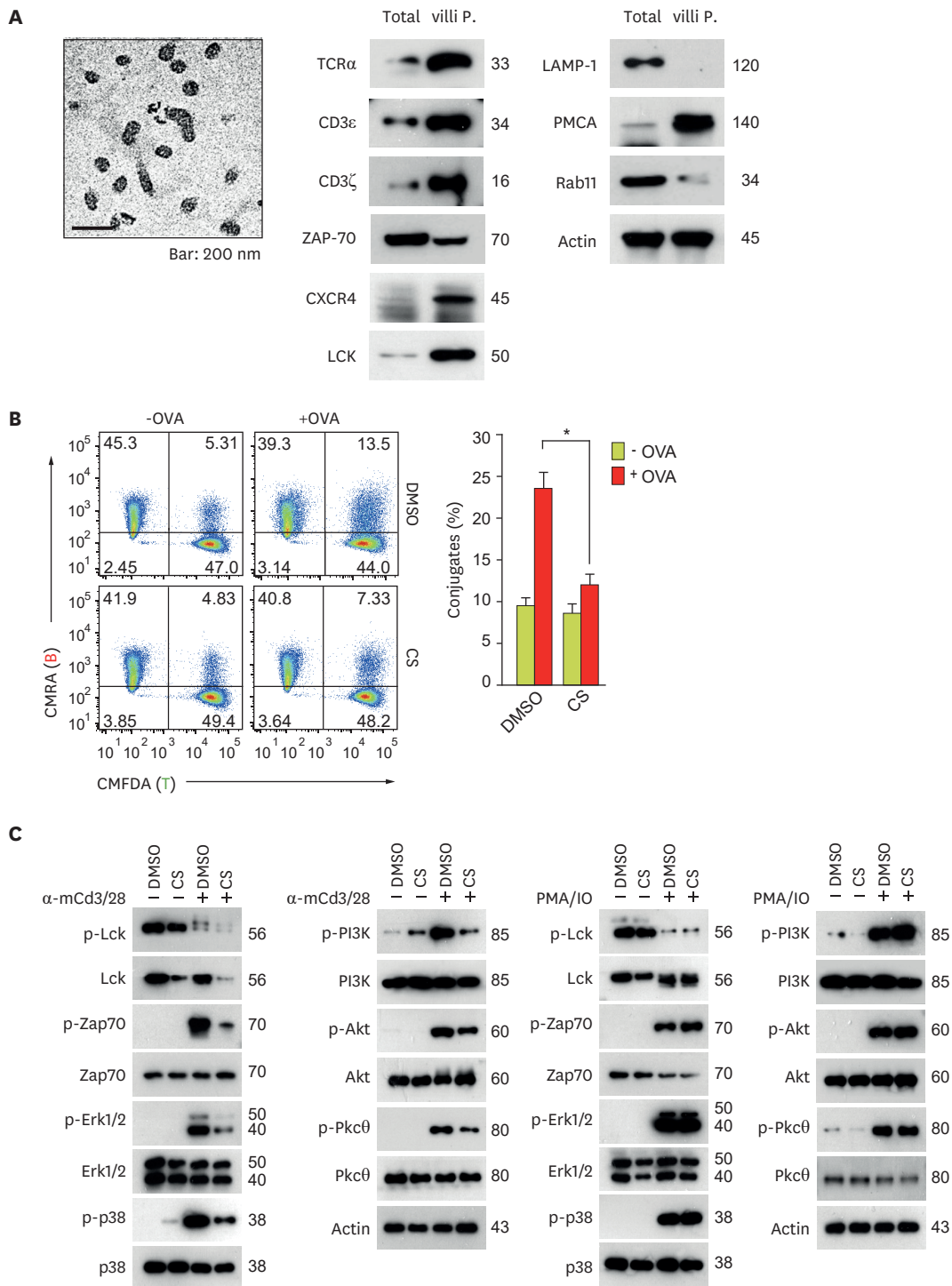
Figure 4. The CS-dependent depletion of T cell microvilli impairs immune responses via TCR signaling.
(A) CD3+ T blasts treated with 100 μM CS for 3 h. Subsequently, shed microvilli particles were harvested and subjected to TEM (left) and Western blotting (right).
(B) CS (100 μM) or vehicle-treated OTII CD4+ T cells stained with CMFDA-green and CD19+ B cells stained with CMRA-orange. Cells were mixed in a 1:1 ratio in the presence or absence of OVA$_{323-339}$ for 1 h, after which the conjugate formation was determined by flow cytometry. (C) Cells were treated as (A), and then washed and stimulated on a α-CD3/28-coated plate or PMA/IO for 30 min. The cells were finally subjected to Western blotting. Results are representative of three independent experiments.
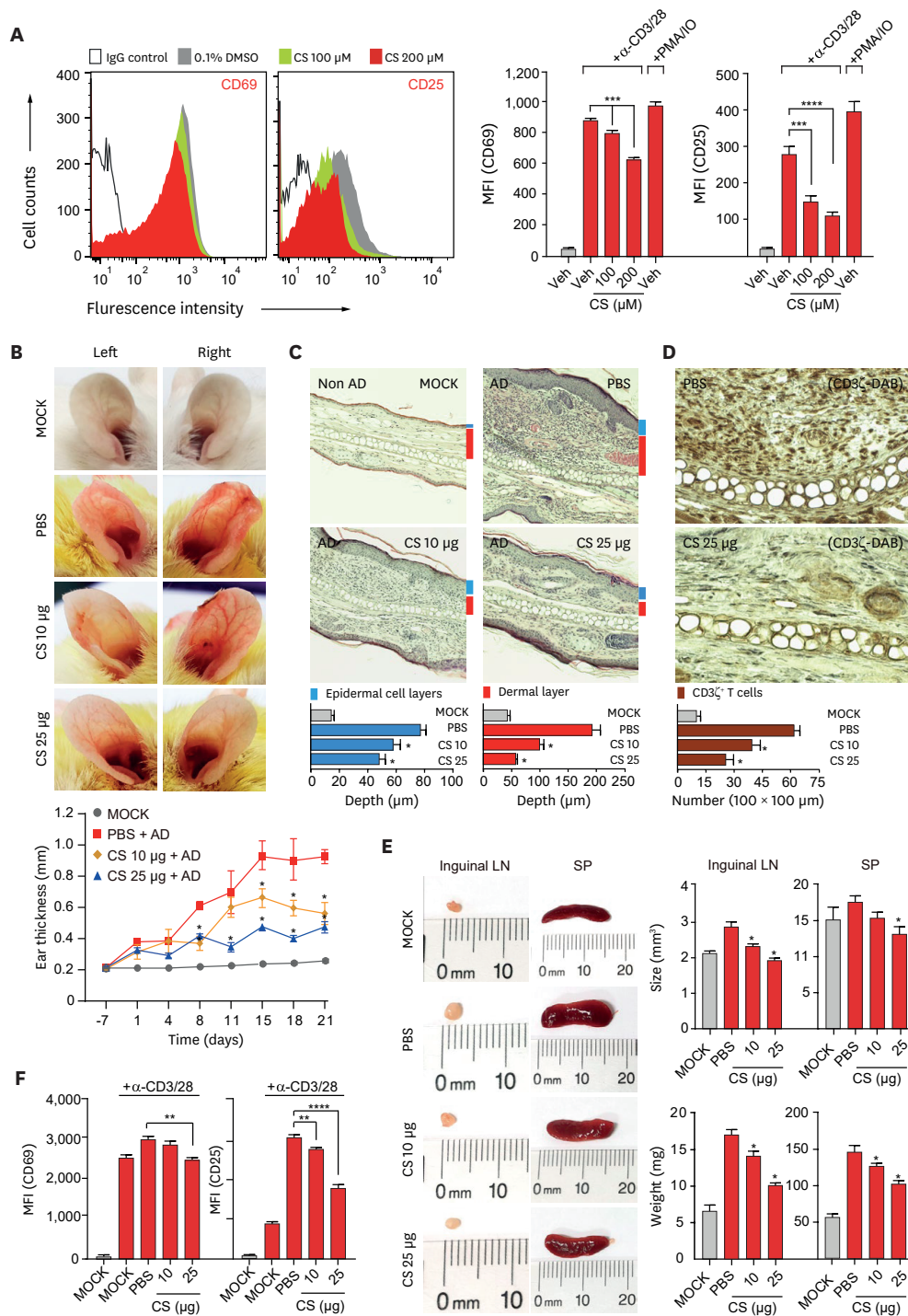Description of footnote mark *.

Figure 5. Immunosuppressive effects of CS on TNBC-induced AD-like symptoms.
(A) Flow cytometric analysis of activated circulating T cell markers after systemic injection of CS *in vivo*. Recipient mice (wild-type BALB/c) were administered 100 or 200 μM of CS thrice every 8 h, and then sacrificed after 24 h from the last injection (n=5). Subsequently, CD3+ T cells were isolated from LNs or spleen, after which the cells were stimulated with an α-CD3/28 Abs or PMA/IO for 8 h. Results are representative of three independent experiments. Data are presented as mean ± SEM. (B-D) Representative pictures of mouse ears (wild-type BALB/c), (B) microphotographs showing H&E staining results, and (C) IHC results from the detection of CD3+ T cells (D) on day 28 post-AD induction. Ear thicknesses were measured at 3-day intervals (n=6). Data are presented as mean ± SD. (E) The size and weight of the inguinal LNs or spleens in the AD-induced mice (n=6) measured at the end of the experiments. Data are presented as mean ± SEM. (F) CD3+ T cells were isolated from LNs of AD-induced mice presented in (E), stimulated with an α-CD3/28 Abs for 8 h, and measured activation marker by flow cytometry (n=6). Data represent mean ± SD. All results (B-D) are quantified for 3 independent AD-induced experiments.
*p<0.05, **p<0.01, ***p<0.001, ****p<0.0001.

post-challenge, however, the severity of AD symptoms including ear swelling and cytokine production was significantly alleviated in the mice adoptively transferred with CD3$^+$ T cells from CS-injected mice, suggesting that CS-treated T cells did not react TNCB and mite in the challenging model (**Fig. 6B-E**). These results provide evidence that CS can attenuate T-cell-mediated immunological diseases such as AD.
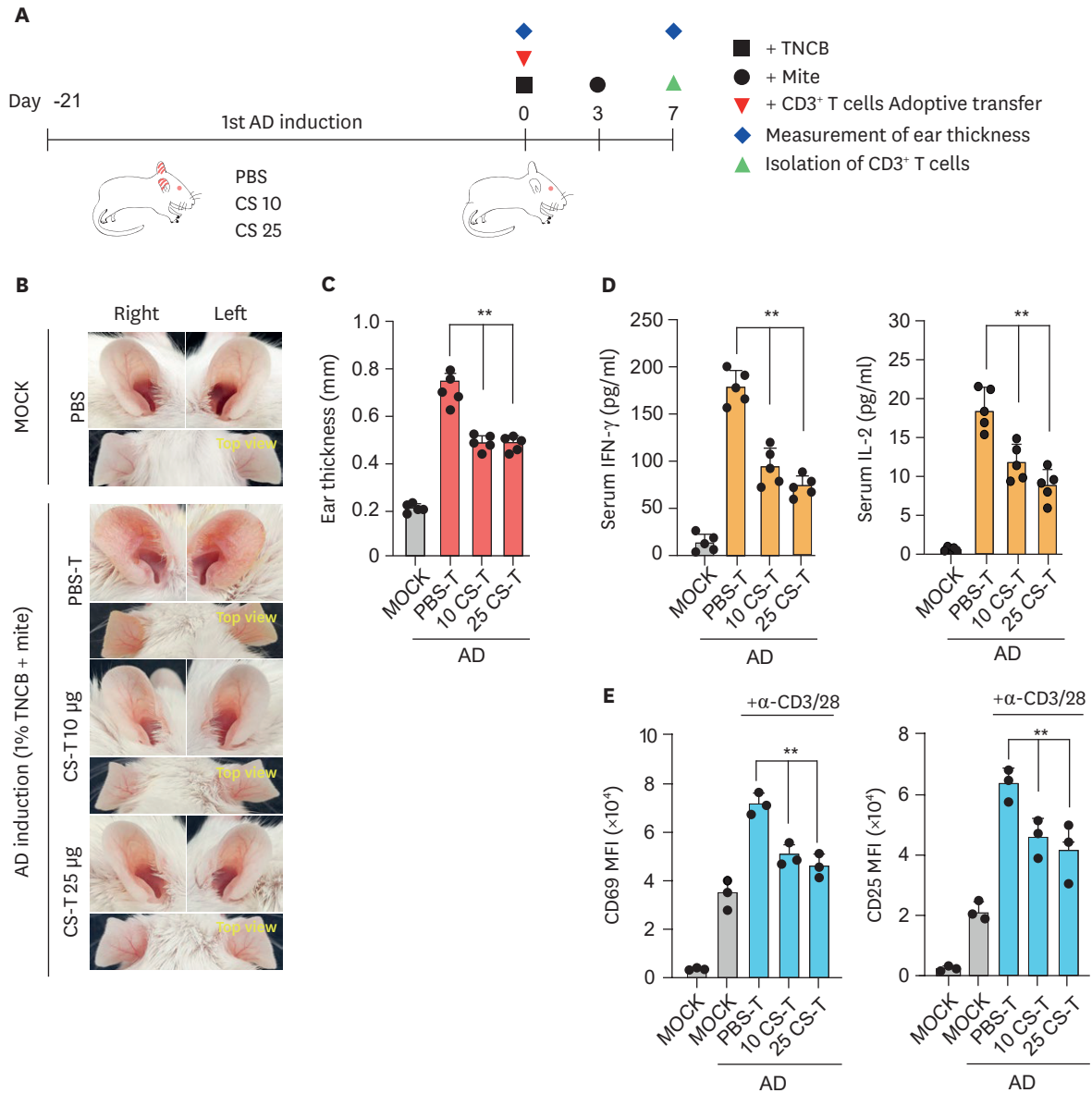

Figure 6. Adoptively transferred CS-treated T cells reduce AD-like symptoms and skin lesions.
(A) Schematic diagram of AD challenge in recipient mice. (B, C) CD3$^+$ T cells from PBS or CS-injected mice isolated from TNCB-sensitized donor mice, followed by treatment of the ears of recipient mice with TNCB and mite after transfer. At day 7, and ear vein and colour were analysed in photographs and ear swelling was determined. Data are shown as the mean ± SEM (n=7) and are representative of 4 experiments. (D) IL-2 and IFN-γ expression in serum from AD-induced recipient mice (day 7). (E) CD69/25 expression for CD3$^+$ T cells isolated from AD-induced recipient mice (day 7). Isolated CD3$^+$ T cells from the recipient mice were stimulated on α-CD3/28 coated plate for 8 h, and CD69/25 expression was measured by using flow cytometry. Data are presented as mean ± SD. **$p<0.01$.

CS leads to the aberrant migration of T cells into the T-cell zone and hampers T cell/DC interactions *in vivo*

Regarding the size differences of the LN and spleen in AD mice and the possibility that microvilli may act as an antenna for searching Ag or chemoattractant, we considered the possibility that CS also affects the migration of T cells. Accordingly, a recent report demonstrated that treatment with CS inhibited the migration of T cells into the eyes (33). Moreover, given that T-cell microvilli also contain proteins, such as CXCR4 and L-selectin (23,24), we hypothesized that T cells exposed to CS have a deficiency in their migration to the secondary lymphoid tissue.

To this end, nontreated and CS-treated T cells were stained with different colors, and then a similar number of cells were injected into recipient mice. Immunofluorescence revealed that T cells treated with CS could not properly migrate to the T-cell zone in the spleen and LN (**Fig. 7A and B**). Based on this finding, we hypothesized that the difference in the migration was due to a defect in the initial adhesion to HEVs and infiltration into the lymphoid tissue. T cells exposed to CS did not properly adhere to HEVs in the LNs, as observed by intra-vital 2-photon microscopy (**Fig. 7C**, **Supplementary Video 2**). Furthermore, using OTII T cells and OVA-pulsed DCs, we confirmed that CS attenuated T cell interaction with DCs *in vivo* (**Fig. 7D**, **Supplementary Videos 3** and **4**). Moreover, cell trace analysis showed that T cells treated with CS could not maintain binding with DC and patrolled inside the lymphoid tissue (**Fig. 7E**). Overall, our results demonstrate that defects in microvilli function caused by endogenous lipid products such as CS can lead to an inappropriate T-cell response, which, to some extent, helps reduce T-cell-dependent immunologic diseases but could be damaging to the host antitumor activity.

DISCUSSION

Most studies related to CL derivatives have been dedicated to investigating metabolic processes. These studies have identified that metabolic processes are diverse and dynamic (8-10). Similarly, given that most CL derivatives are lipophilic, a lipid carrier such as a low-density lipoprotein (LDL) receptor is essential for transport in the blood (34). CS, for example, behaves differently due to its sulfate group, which has an electric charge that helps it move unperturbed through the bloodstream (13). As a result, CS is a CL derivative that is abundantly present in human plasma (approximately 3 µg/ml) (15,35). Studies have also suggested that CS can have systemic effects while circulating in the blood. From this viewpoint, peripheral blood cells could be targets for the influence of circulating CS. Furthermore, increased CS concentrations in the blood have considerably been associated with diseases like X-linked ichthyosis (36), hypothyroidism (37), and cirrhosis of the liver (38). However, it is largely unverified whether CS can regulate immunologic diseases like AD, rheumatoid arthritis, and colitis.

We showed here that the membrane expression of TCRs was substantially decreased in T cells treated with CS. Interestingly, the decreased expression of TCRs was associated with the release of microvilli particles. Previously, Wang et al. (22) reported that CS disrupts TCR microclusters, which may affect the reduction of the immune response. In contrast, our results revealed that the reduction in TCR clusters by CS depended on the release of the microvilli in which the TCRs were enriched (23,24). Additionally, using CS, a previous study reported the loss of microvilli-specific proteins, CD62L and CD44, which further corroborates that
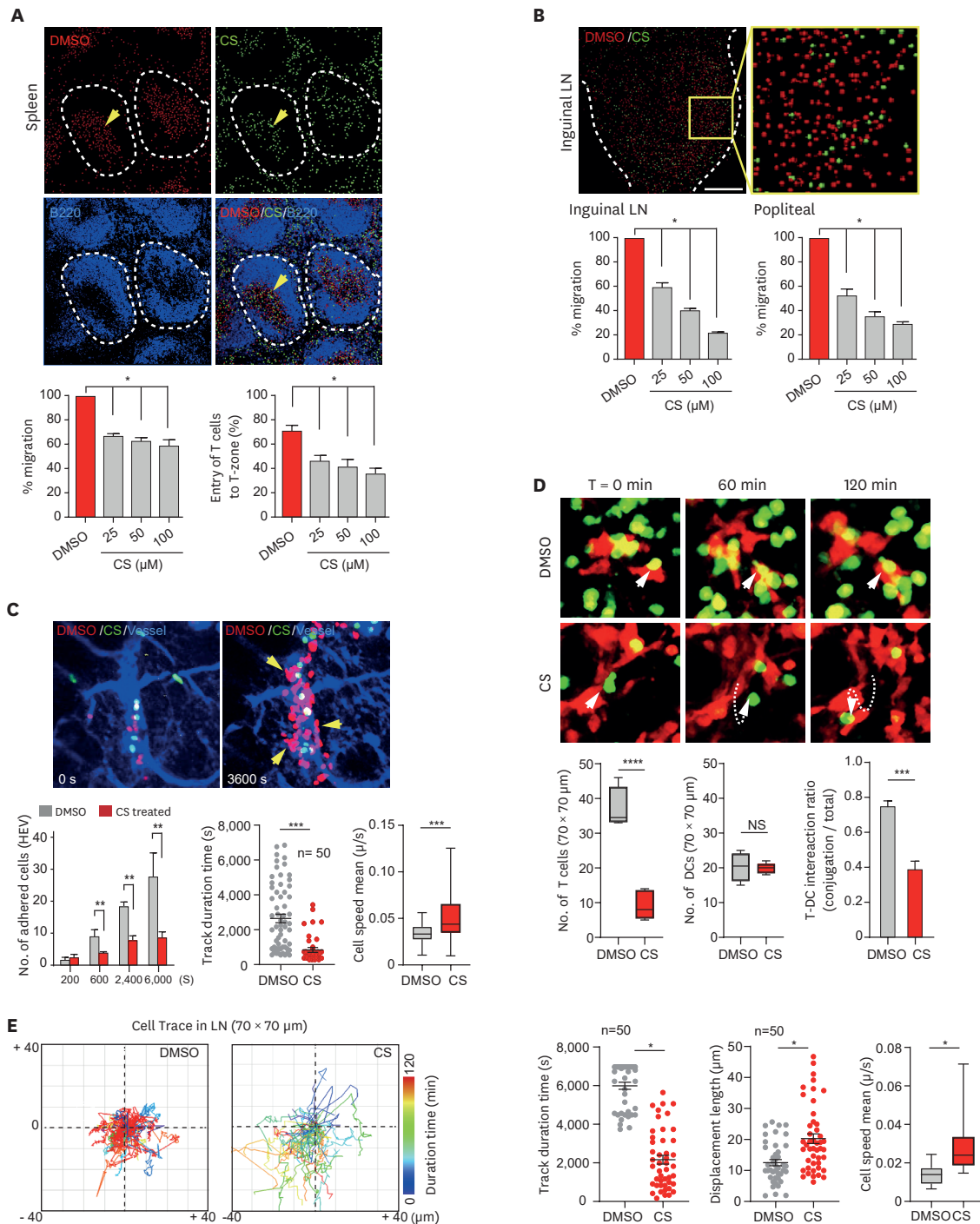
Figure 7. The presence of excessive CS perturbs the migration of T cells to secondary lymphoid organs.
(A, B) Naïve CD3^{+} T cells treated with CS (100 μM) or a vehicle for 3 h, and then stained with CMFDA-green or CMRA-orange. The labeled cells were adoptively transferred to recipient mice (wild-type C57BL/6) i.v. at a 1:1 ratio. At 24 h post-injection, the number of migratory cells in the spleen (A) or inguinal LN (B) was analyzed using fixed cryosections (n=5). (C) Representative snapshots of live HEV binding images, showing CD3^{+} T cells treated with CS (100 μM) or the vehicle. A popliteal LN was immediately imaged using 2-photon microscopy after injection of T cells (n=3). (D) Representative snapshot of live DC-T cell interaction images *in vivo*. OVA$_{323-339}$ (1 μg/mL)-pulsed BMDCs (5×10^6) were stained with Cell Tracker CMRA-orange and injected s.c. into the footpads of recipient mice (n=3). At 24 h post-injection, CS- (100 μM) or vehicle-treated OTII CD4^{+} T cells were also stained with CMFDA-green and adoptively transferred to recipient mice i.v. Subsequently, two-photon microscopy visualized the draining popliteal LNs at 24 h post-injection. White arrowheads indicate the contact cells, and the dotted line represents the indicated cell trace. Statistical analysis results of the number of T cells, DCs, and T-DC interaction ratio are presented (scale bar=10 μm). (E) The trajectory of T cells in each group presented in (D) (n=50). All images were analyzed using the Imaris 8.0 software, and statistical analysis results were presented. All results represent 3 independent experiments, and data are presented as mean ±SEM.
*p<0.05, **p<0.01, ***p<0.001, ****p<0.0001.

CS affects T-cell microvilli (23,24). However, in this study, T cells with a reduced number of microvilli by CS showed a severe defect in TCR-mediated signaling compared with that in untreated T cells. The conjugation strength and dwelling time with APCs was also poor *in vitro* and *in vivo*. These results show that microvilli are important membrane protrusive structures that recognize Ags and initiate Ag-specific T cell responses (39).

The next question was how CS collapsed the microvilli. We observed that the selective extraction of CL by MβCD induced a reduction in microvilli, which was largely recoverable by CL supplementation. In contrast, microvilli collapse by CS was not recovered by CL, suggesting that CS and CL compete with each other based on the microvilli constitution. These results further show that people with high extracellular CL concentrations or hypercholesterolemia may be less sensitive to the effects of CS in their blood. Otherwise, increased concentrations of circulating CS in the blood may attenuate immune responses such as T-cell-mediated delayed hypersensitivity. Nevertheless, increased blood levels of CS by injecting CS into the blood vessels of mice substantially reduced the activation of T cells purified from those mice.

A dramatic reduction in atopic lesions by CS application suggests that CS reduces T cell responses *in vivo*. However, T cells obtained from CS-injected mice did not show a significant difference in the number and length of microvilli. This finding may imply that only small changes in microvilli constitution result in significant changes *in vivo*. Accordingly, CS effectively suppressed the hyper-activation of immune responses in the AD model, proposing that AD suppression was related to the reduced migration and homing of T cells into atopic lesions, spleen, and LNs. Previously, Sakurai et al. (33) reported a defect in the migration of CS-treated T cells *in vitro* and the easing of eye inflammation. Interestingly, certain cancer cells such as colon and prostate cancers also produce CS abundantly (40,41). Moreover, the level of CS is inversely correlated with the extent of CD8^{+} T cell infiltration in cancer tissue (40). Thus, the pharmacologic or molecular intervention of CS-mediated T-cell exclusion could be a good strategy for promoting antitumor activity in patients (42).

Although reports, but not many, have emphasized the importance of T-cell microvilli in T cell functions (23-25), our report is the first evidence that microvilli defects in T cells by CS suppress T cell-dependent immune reactions and diseases. Besides, given that the microvilli collapse by CS is reversible (**Supplementary Fig. 4**), intermittent exposure to CS may effectively control T cell-dependent diseases. Therefore, CS is proposed as a promising therapeutic for T cell-dependent autoimmune diseases, including AD, rheumatoid arthritis, and colitis.

ACKNOWLEDGEMENTS

![Immune Network logo]

SUPPLEMENTARY MATERIALS

Supplementary Figure 1
A short-term exposure of CS reduces the expression of microvilli-enriched proteins on T cell surface.

Click here to view

Supplementary Figure 2
External CS collapses lipid rafts and depletes membrane CL.

Click here to view

Supplementary Figure 3
Filopodyan analyses of scanning electron microscopy images. Each cell's microvilli/2D outline was measured using Image J-Filopodyan (S1). Representative images of the Filopodyan quantitation process of each cell treated with 0.1% DMSO, 100 μM CS, and 50 mM MβCD is also shown.

Click here to view

Supplementary Figure 4
The microvilli in CS-treated T cells recovered from fresh media.

Click here to view

Supplementary Figure 5
Schematic showing the TNBC-induced AD mouse model and administration of CS in BALB/c mice.

Click here to view

Supplementary Video 1
Defective centripetal movements of CS-treated T cells in the lipid bilayer. OTII CD4$^+$ T blasts were treated with CS (100 μM) or the vehicle for 3 h, and then stained with TCRβ (H57Fab-594). Subsequently, the cells were placed on a planar lipid bilayer presenting OVA$_{323-339}$-I-A^b/ICAM-1, and then immediately imaged for 30 min every 15 s under TIRFM. Relative time scales starting from the moment of cell spreading are labeled in the movie. This video corresponds to **Fig. 2B**.

Click here to view

Supplementary Video 2
Defective T cell homing into the secondary organs of CS-treated cells. Naive CD3$^+$ T cells were treated with CS (100 μM) or the vehicle for 3 h, and then stained with CMFDA or CMRA for 30 min at 37°C, respectively. Subsequently, the labeled cells were mixed at a 1:1 ratio in 200 μl dextran, Cascade Blue™, followed by an adoptive transfer to recipient mice i.v. After being injected, the homing and cellular traffic of T cells in the LN were imaged for 2 h using a Zeiss LSM 880 microscope.

Click here to view

Supplementary Video 3

Normal T cell interaction with Ag-loaded DCs in vehicle-treated T cells at the popliteal LN. OVA (323–339, 1 µg/ml)-pulsed BMDCs ($5×10^6$) were stained with Cell Tracker CMRA-orange and injected s.c. into the footpads of recipient mice. At 24 h post-injection, vehicle-treated OTII CD4^{+} T cells were stained with CMFDA-green and adoptively transferred to recipient mice i.v. with 200 µl dextran. Cells at the popliteal LN were finally imaged using a Zeiss LSM 880 microscope for 2 h.

Click here to view

Supplementary Video 4

Defective T cell interaction with Ag-loaded DCs in CS-treated T cells at the popliteal LN. OVA (323–339, 1 µg/ml)-pulsed BMDCs ($5×10^6$) were stained with Cell Tracker CMRA-orange and injected s.c. into the footpads of recipient mice. At 24 h post-injection, 100 µM CS-treated OTII CD4^{+} T cells were stained with CMFDA-green and adoptively transferred to recipient mice i.v. with 200 µl dextran. Cells at the popliteal LN were finally imaged using a Zeiss LSM 880 microscope for 2 h.

Click here to view

REFERENCES

1. Cooper RA. Influence of increased membrane cholesterol on membrane fluidity and cell function in human red blood cells. *J Supramol Struct* 1978;8:413-430.
   PUBMED | CROSSREF

2. Roberts KD, Bandi L, Calvin HI, Drucker WD, Lieberman S. Evidence that cholesterol sulfate is a precursor of steroid hormones. *J Am Chem Soc* 1964;86:958-959.
   CROSSREF

3. Mansour S, Tocheva AS, Cave-Ayland C, Machelett MM, Sander B, Lissin NM, Molloy PE, Baird MS, Stübs G, Schröder NW, et al. Cholesteryl esters stabilize human CD1c conformations for recognition by self-reactive T cells. *Proc Natl Acad Sci U S A* 2016;113:E1266-E1275.
   PUBMED | CROSSREF

4. Brown DA, London E. Structure and origin of ordered lipid domains in biological membranes. *J Membr Biol* 1998;164:103-114.
   PUBMED | CROSSREF

5. Molnár E, Swamy M, Holzer M, Beck-García K, Worch R, Thiele C, Guigas G, Boye K, Luescher IF, Schwille P, et al. Cholesterol and sphingomyelin drive ligand-independent T-cell antigen receptor nanoclustering. *J Biol Chem* 2012;287:42664-42674.
   PUBMED | CROSSREF

6. Larbi A, Douziech N, Khalil A, Dupuis G, Gheraïri S, Guérard KP, Fülöp T Jr. Effects of methyl-β-cyclodextrin on T lymphocytes lipid rafts with aging. *Exp Gerontol* 2004;39:551-558.
   PUBMED | CROSSREF

7. Kabouridis PS, Janzen J, Magee AL, Ley SC. Cholesterol depletion disrupts lipid rafts and modulates the activity of multiple signaling pathways in T lymphocytes. *Eur J Immunol* 2000;30:954-963.
   PUBMED | CROSSREF

8. Kulig W, Cwiklik L, Jurkiewicz P, Rog T, Vattulainen I. Cholesterol oxidation products and their biological importance. *Chem Phys Lipids* 2016;199:144-160.
   PUBMED | CROSSREF

9. Ren S, Ning Y. Sulfation of 25-hydroxycholesterol regulates lipid metabolism, inflammatory responses, and cell proliferation. *Am J Physiol Endocrinol Metab* 2014;306:E123-E130.
   PUBMED | CROSSREF

10. Nguyen TM, Sawyer JK, Kelley KL, Davis MA, Rudel LL. Cholesterol esterification by ACAT2 is essential for efficient intestinal cholesterol absorption: evidence from thoracic lymph duct cannulation. *J Lipid Res* 2012;53:95-104.
    PUBMED | CROSSREF

11. Gold ES, Diercks AH, Podolsky I, Podyminogin RL, Askovich PS, Treuting PM, Aderem A. 25-Hydroxycholesterol acts as an amplifier of inflammatory signaling. *Proc Natl Acad Sci U S A* 2014;111:10666-10671.
PUBMED | CROSSREF

12. Ryan L, O'Callaghan YC, O'Brien NM. The role of the mitochondria in apoptosis induced by 7β-hydroxycholesterol and cholesterol-5β,6β-epoxide. *Br J Nutr* 2005;94:519-525.
PUBMED | CROSSREF

13. Javitt NB, Lee YC, Shimizu C, Fuda H, Strott CA. Cholesterol and hydroxycholesterol sulfotransferases: identification, distinction from dehydroepiandrosterone sulfotransferase, and differential tissue expression. *Endocrinology* 2001;142:2978-2984.
PUBMED | CROSSREF

14. Bleau G, Bodley FH, Longpré J, Chapdelaine A, Roberts KD. Cholesterol sulfate. I. Occurrence and possible biological function as an amphipathic lipid in the membrane of the human erythrocyte. *Biochim Biophys Acta* 1974;352:1-9.
PUBMED | CROSSREF

15. Drayer NM, Lieberman S. Isolation of cholesterol sulfate from human blood and gallstones. *Biochem Biophys Res Commun* 1965;18:126-130.
PUBMED | CROSSREF

16. Hanley K, Wood L, Ng DC, He SS, Lau P, Moser A, Elias PM, Bikle DD, Williams ML, Feingold KR. Cholesterol sulfate stimulates involucrin transcription in keratinocytes by increasing Fra-1, Fra-2, and Jun D. *J Lipid Res* 2001;42:390-398.
PUBMED | CROSSREF

17. Roberts KD. Sterol sulfates in the epididymis; synthesis and possible function in the reproductive process. *J Steroid Biochem* 1987;27:337-341.
PUBMED | CROSSREF

18. Langlais J, Zollinger M, Plante L, Chapdelaine A, Bleau G, Roberts KD. Localization of cholesteryl sulfate in human spermatozoa in support of a hypothesis for the mechanism of capacitation. *Proc Natl Acad Sci U S A* 1981;78:7266-7270.
PUBMED | CROSSREF

19. Iwamori M, Iwamori Y, Ito N. Regulation of the activities of thrombin and plasmin by cholesterol sulfate as a physiological inhibitor in human plasma. *J Biochem* 1999;125:594-601.
PUBMED | CROSSREF

20. Bleau G, Chapdelaine A, Roberts KD. The assay of cholesterol sulfate in biological material by enzymatic radioisotopic displacement. *Can J Biochem* 1972;50:277-286.
PUBMED | CROSSREF

21. Cheetham JJ, Epand RM, Andrews M, Flanagan TD. Cholesterol sulfate inhibits the fusion of Sendai virus to biological and model membranes. *J Biol Chem* 1990;265:12404-12409.
PUBMED | CROSSREF

22. Wang F, Beck-García K, Zorzin C, Schamel WW, Davis MM. Inhibition of T cell receptor signaling by cholesterol sulfate, a naturally occurring derivative of membrane cholesterol. *Nat Immunol* 2016;17:844-850.
PUBMED | CROSSREF

23. Jung Y, Riven I, Feigelson SW, Kartvelishvily E, Tohya K, Miyasaka M, Alon R, Haran G. Three-dimensional localization of T-cell receptors in relation to microvilli using a combination of superresolution microscopies. *Proc Natl Acad Sci U S A* 2016;113:E5916-E5924.
PUBMED | CROSSREF

24. Kim HR, Mun Y, Lee KS, Park YJ, Park JS, Park JH, Jeon BN, Kim CH, Jun Y, Hyun YM, et al. T cell microvilli constitute immunological synaptosomes that carry messages to antigen-presenting cells. *Nat Commun* 2018;9:3630-3648.
PUBMED | CROSSREF

25. Cai E, Marchuk K, Beemiller P, Beppler C, Rubashkin MG, Weaver VM, Gérard A, Liu TL, Chen BC, Betzig E, et al. Visualizing dynamic microvillar search and stabilization during ligand detection by T cells. *Science* 2017;356:eaal3118.
PUBMED | CROSSREF

26. Labrecque N, Whitfield LS, Obst R, Waltzinger C, Benoist C, Mathis D. How much TCR does a T cell need? *Immunity* 2001;15:71-82.
PUBMED | CROSSREF

27. Takeuchi Y, Hirota K, Sakaguchi S. Impaired T cell receptor signaling and development of T cell-mediated autoimmune arthritis. *Immunol Rev* 2020;294:164-176.
PUBMED | CROSSREF

28. Huang JF, Yang Y, Sepulveda H, Shi W, Hwang I, Peterson PA, Jackson MR, Sprent J, Cai Z. TCR-Mediated internalization of peptide-MHC complexes acquired by T cells. *Science* 1999;286:952-954.
PUBMED | **CROSSREF**

29. Poole K, Meder D, Simons K, Müller D. The effect of raft lipid depletion on microvilli formation in MDCK cells, visualized by atomic force microscopy. *FEBS Lett* 2004;565:53-58.
PUBMED | **CROSSREF**

30. Ikenouchi J, Hirata M, Yonemura S, Umeda M. Sphingomyelin clustering is essential for the formation of microvilli. *J Cell Sci* 2013;126:3585-3592.
PUBMED | **CROSSREF**

31. Marzesco AM, Wilsch-Bräuninger M, Dubreuil V, Janich P, Langenfeld K, Thiele C, Huttner WB, Corbeil D. Release of extracellular membrane vesicles from microvilli of epithelial cells is enhanced by depleting membrane cholesterol. *FEBS Lett* 2009;583:897-902.
PUBMED | **CROSSREF**

32. Choudhuri K, Llodrá J, Roth EW, Tsai J, Gordo S, Wucherpfennig KW, Kam LC, Stokes DL, Dustin ML. Polarized release of T-cell-receptor-enriched microvesicles at the immunological synapse. *Nature* 2014;507:118-123.
PUBMED | **CROSSREF**

33. Sakurai T, Uruno T, Sugiura Y, Tatsuguchi T, Yamamura K, Ushijima M, Hattori Y, Kukimoto-Niino M, Mishima-Tsumagari C, Watanabe M, et al. Cholesterol sulfate is a DOCK2 inhibitor that mediates tissue-specific immune evasion in the eye. *Sci Signal* 2018;11:eaao4874.
PUBMED | **CROSSREF**

34. Brown MS, Goldstein JL. Lipoprotein receptors in the liver. Control signals for plasma cholesterol traffic. *J Clin Invest* 1983;72:743-747.
PUBMED | **CROSSREF**

35. Strott CA, Higashi Y. Cholesterol sulfate in human physiology: what's it all about? *J Lipid Res* 2003;44:1268-1278.
PUBMED | **CROSSREF**

36. Epstein EH JrKrauss RM, Shackleton CH. X-linked ichthyosis: Increased blood cholesterol sulfate and electrophoretic mobility of low-density lipoprotein. *Science* 1981;214:659-660.
CROSSREF

37. van Doormaal JJ, Muskiet FA, Jansen G, Wolthers BG, Sluiter WJ, Doorenbos H. Increase of plasma and red cell cholesterol sulfate levels in induced hypothyroidism in man. *Clin Chim Acta* 1986;155:195-200.
PUBMED | **CROSSREF**

38. Tamasawa N, Tamasawa A, Takebe K. Higher levels of plasma cholesterol sulfate in patients with liver cirrhosis and hypercholesterolemia. *Lipids* 1993;28:833-836.
PUBMED | **CROSSREF**

39. Takeuchi K, Sato N, Kasahara H, Funayama N, Nagafuchi A, Yonemura S, Tsukita S, Tsukita S. Perturbation of cell adhesion and microvilli formation by antisense oligonucleotides to ERM family members. *J Cell Biol* 1994;125:1371-1384.
PUBMED | **CROSSREF**

40. Tatsuguchi T, Uruno T, Sugiura Y, Sakata D, Izumi Y, Sakurai T, Hattori Y, Oki E, Kubota N, Nishimoto K, et al. Cancer-derived cholesterol sulfate is a key mediator to prevent tumor infiltration by effector T cells. *Int Immunol* 2022;34:277-289.
PUBMED | **CROSSREF**

41. Eberlin LS, Dill AL, Costa AB, Ifa DR, Cheng L, Masterson T, Koch M, Ratliff TL, Cooks RG. Cholesterol sulfate imaging in human prostate cancer tissue by desorption electrospray ionization mass spectrometry. *Anal Chem* 2010;82:3430-3434.
PUBMED | **CROSSREF**

42. Tatsuguchi T, Uruno T, Sugiura Y, Oisaki K, Takaya D, Sakata D, Izumi Y, Togo T, Hattori Y, Kunimura K, et al. Pharmacological intervention of cholesterol sulfate-mediated T cell exclusion promotes antitumor immunity. *Biochem Biophys Res Commun* 2022;609:183-188.
PUBMED | **CROSSREF**